

1 **Characterizing water solubility of fresh and aged secondary organic**
2 **aerosol in PM_{2.5} with the stable carbon isotope technique**

3

4 Fenghua Wei¹, Xing Peng¹, Liming Cao¹, Mengxue Tang¹, Ning Feng¹, Xiaofeng Huang¹, Lingyan
5 He¹

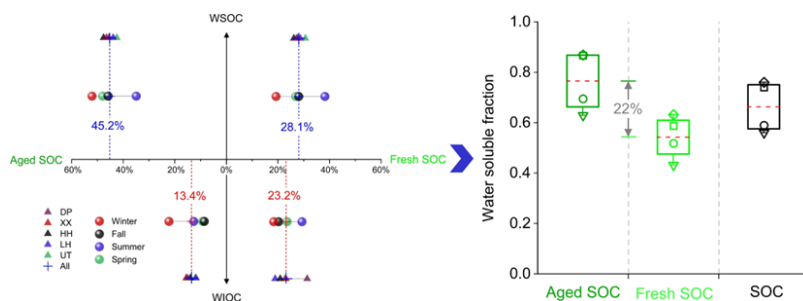
6 ¹Laboratory of Atmospheric Observation Supersite, School of Environment and Energy, Peking
7 University Shenzhen Graduate School, Shenzhen 518055, China.

8 **Correspondence:** Xing Peng (pengxing@pku.edu.cn)

9 **Abstract:** The investigation of the water-soluble characteristics of secondary organic carbon (SOC) is
 10 essential for a more comprehensive understanding of its climate effects. However, due to the
 11 limitations of the existing source apportionment methods, the water solubility of different types of SOC
 12 remains uncertain. This study analyzed stable carbon isotope and mass spectra signatures of total
 13 carbon (TC) and water-soluble organic carbon (WSOC) in ambient PM_{2.5} samples for one year and
 14 established stable carbon isotope profiles of fresh and aged SOC. Furthermore, the Bayesian stable
 15 isotope mixing (BSIM) model was employed to reveal the water solubility characteristics of fresh and
 16 aged SOC in a coastal megacity of China. WSOC was dominated by secondary sources, with fresh and
 17 aged SOC contributing 28.1 % and 45.2 %, respectively. Water-insoluble organic carbon (WIOC) was
 18 dominated by primary sources, to which fresh and aged SOC contributed 23.2 % and 13.4 %. We also
 19 found the aging degree of SOC has considerable impacts on its water solubility due to the much higher
 20 water-soluble fraction of aged SOC (76.5 %) than fresh SOC (54.2 %). Findings of this study may
 21 provide a new perspective for further investigation of the hygroscopicity effects of SOC with different
 22 aging degrees on light extinction and climate change.

23 **Keywords:** Fresh SOC; Aged SOC; Water solubility; Stable carbon isotope; BSIM model; Mass
 24 spectrometry.

25 **Graphical abstract:**



26

27 **1. Introduction**

28 As a major component of particulate matter (PM_{2.5}), secondary organic aerosols (SOA) not only
29 contribute to haze formation but also exert a substantial influence on climate dynamics across various
30 spatial scales, from local to global (Kaul et al., 2011; Shrivastava et al., 2017). The water solubility,
31 considered one of the crucial physical properties of SOA, has been extensively studied recently due to
32 its significant effects on the physicochemical processes in the atmosphere. The water solubility of SOA
33 varied with its aging degrees (Kirillova et al., 2013), while both the water solubility and aging degree
34 of organic aerosols contribute to the hygroscopicity noticeably, which affects the light extinction
35 eventually (Han et al., 2022; Liu et al., 2022). Hence, exploring the water solubility characteristics of
36 SOA with different aging degrees can help elucidate the more detailed extinction mechanism of SOA.
37 In addition, recent studies have also shown that the formation of secondary particulates is one of the
38 main processes determining the amount of ~~cloud condensation nuclei (CCN)~~ in remote oceanic regions
39 (Liu and Matsui 2022). Therefore, investigating the water solubility of SOA with different aging
40 degrees is also meaningful for further exploring its indirect climate effects.

Deleted: CCN

41 Investigating the contributions of SOA with different aging degrees to both organic matter (OM)
42 and water-soluble organic matter (WSOM) is imperative for determining their quantified water
43 solubility. However, due to the constraints of reliable methods, only a limited number of studies have
44 examined the water solubility of SOA using mass spectrometry techniques. Qiu et al. (2019) conducted
45 source apportionment of OM in PM₁ and WSOM in PM_{2.5} based on online and offline AMS-PMF
46 methods respectively (Qiu et al., 2019). This approach faces challenges not only related to the inherent
47 errors of online versus offline methods but also discrepancies in the measured particle sizes of OM and
48 WSOM. Kondo et al. (2007) and Timonen et al. (2013) attempted to apportion water-soluble organic

50 carbon (WSOC) through a multiple linear regression method based on the mass spectral information of
51 OM, which still exhibits large indeterminateness (Timonen et al., 2013; Xiao et al., 2011; Kondo et al.,
52 2007). The carbon isotopic technique offers a promising avenue to overcome the aforementioned
53 limitations, thereby enabling a more in-depth exploration of the water-soluble characteristics of SOA.
54 Carbon isotope techniques have garnered widespread attention and are increasingly employed in source
55 apportionment studies of organic aerosols due to their robust source appointment capabilities.
56 Radioactive carbon isotopes (^{14}C) provide a precise method for quantitatively distinguishing between
57 fossil and non-fossil organic aerosol sources (Fushimi et al., 2011; Zhang et al., 2014). The stable
58 carbon isotope technique (^{13}C), however, can quantitatively assess the contributions of various sources
59 by integrating them into mass balance models (Yao et al., 2022; Widory et al., 2004). The Bayesian
60 mixing model stands out as one of the most widely utilized models (Xiao;Xu and Xiao 2023; Tang et
61 al., 2020). The stable carbon isotope technique can also be combined with other source tracers to
62 further enhance the accuracy of source apportionment of carbonaceous aerosols (Jiang et al., 2022;
63 Plasencia Sánchez et al., 2023; Ceburnis et al., 2011; Lim et al., 2022). However, to our knowledge, no
64 study has employed the carbon isotope technique to estimate the source contribution of both fresh and
65 aged SOA before, owing to the challenging measurement of the carbon isotope profiles for these two
66 sources.

67 Previous studies have predominantly concentrated on assessing the water solubility of SOA at
68 inland urban sites, revealing a strong correlation between SOA water solubility and urban air pollution
69 emissions as well as relative humidity (Wong;Zhou and Abbatt 2015; Pye et al., 2017; Favez et al.,
70 2008; Salma et al., 2007; Weber et al., 2007; Miyazaki et al., 2006). Nevertheless, few researchers have
71 noticed the differences between inland and coastal cities. As dynamic interfaces between urban and

72 marine environments (Donaldson and George 2012), coastal cities exhibit unique characteristics.
73 Shenzhen is a typical representative city for coastal air pollution studies with a coastline spanning
74 260.5 km and a total sea area of 1145 m². We measured the stable carbon isotope fingerprints of fresh
75 and aged secondary organic carbon (SOC), which enables us to investigate the source contributions of
76 SOC with different aging degrees to WSOC and their respective water solubility in Shenzhen.

Deleted: end-members

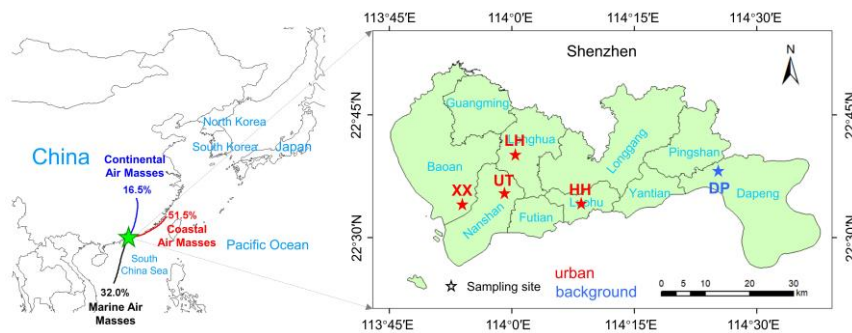
77 The aim of this study is to investigate the water solubility of SOC in PM_{2.5}, emphasizing Shenzhen
78 as a representative mega-coastal city in China. We analyzed stable carbon isotopes and mass spectra
79 signatures of total carbon (TC) and WSOC in ambient PM_{2.5} samples that were collected from five
80 distinct sites in Shenzhen over one year as well as specific emission sources. For the first time, we
81 employed the Bayesian stable isotope mixing (BSIM) model on localized source profiles to quantify
82 the contributions of fresh SOC and aged SOC to WSOC and water-insoluble organic carbon (WIOC).
83 These results would contribute to estimating the water solubility of both fresh and aged SOC, revealing
84 their direct or indirect implications for climate change.

85 2. Material and methods

86 2.1 Ambient PM_{2.5} sampling and chemical analysis

87 Shenzhen (N22°27' ~ N22°52', E113°46' ~ E114°37'), one megacity of Pearl River Delta, China, is
88 bordered by Daya Bay and Dapeng Bay to the east, the Pearl River Estuary and Lingding Sea to the
89 west, Hong Kong to the south, and Dongguan and Huizhou to the north. As a typical mega-coastal city
90 in China, Shenzhen's air quality is predominantly affected by the continental air mass from northern
91 Guangdong, the eastern coastal air mass, and the southern marine air mass (Fig. 1). For a
92 comprehensive exploration of pollution characteristics in Shenzhen, PM_{2.5} samples were collected from

94 five sites covering the western to eastern regions of the city. The selected sites are Xixiang (XX, urban
 95 site), University Town (UT, urban site), Longhua (LH, urban site), Honghu (HH, urban site), and
 96 Dapeng (DP, background site) (Fig. 1). Additional details about each sampling site are listed in Table
 97 S1.



98

99 **Figure 1.** Spatial distribution of the five sampling sites in Shenzhen for this study.

100 In this study, 24-hour $PM_{2.5}$ sampling was conducted every other day in 2019 at the UT site using
 101 a Thermo 2300 atmospheric particulate sampler (Thermo Fisher Scientific Inc., Waltham,
 102 Massachusetts, USA), yielding a total of 160 valid samples. For the remaining four sites, a total of 295
 103 valid $PM_{2.5}$ samples were collected every other day during typical months of the four seasons in 2019
 104 (March, June, September, and December, Table S2) using a Model TH-16A atmospheric particulate
 105 sampler (Tianhong Corp., Wuhan, China). The $PM_{2.5}$ samples collected by the quartz filter were used to
 106 determine the organic carbon (OC) and elemental carbon (EC) using an OC/EC analyzer (2001A,
 107 Desert Research Institute, Reno, Nevada, USA) following the IMPROVE A procedure. In addition, the
 108 samples collected by Teflon filter in this study were analyzed for water-soluble ions (mainly SO_4^{2-} ,
 109 NO_3^- , NH_4^+ , and Cl^-) within $PM_{2.5}$, and the mass concentrations of twenty-three metallic elements
 110 (primarily Na, Mg, Al, K, Ca, V, Fe, Ni, Zn, Pb, and Cd) within $PM_{2.5}$ were also determined using an

111 [inductively coupled plasma mass spectrometer \(ICP-MS, Aurora M90; Bruker, Germany\). Relevant](#)
112 [quality control information is described in the Supplementary Information \(Text S1\).](#)

113 For WSOC extraction, the PM_{2.5} sample underwent ultrasonication (20 min × 3 times) in 15 ml
114 ultrapure water (18.2 MΩ·cm), followed by filtration through a syringe with a 0.45 μm filter head to
115 eliminate insoluble particles. The extracted PM_{2.5} samples were sequentially analyzed using a long-
116 time-of-flight aerosol mass spectrometer (L-TOF-AMS, Aerodyne, USA) and an ultrasonic nebulizer
117 (U5000AT+, Cetac Technologies Inc., USA) to measure elemental ratios, such as O/C, as well as the
118 mass spectrum signatures of the water-soluble organic fractions, including ion fragments like CO₂⁺,
119 C₄H₉⁺, and C₂H₄O₂⁺. The concentration of WSOC was determined using a total organic carbon analyzer
120 (multi N/C 3100, Jena, Germany), and WIOC was calculated as the difference between OC and WSOC.

121 To investigate the stable carbon isotope signatures of carbonaceous aerosols, we built a stable
122 isotope spectrometry system by integrating an OC/EC analyzer with a carbon dioxide isotope
123 spectrometer (QCLAS, Aerodyne). This system reduces the carbon requirement for isotope analysis
124 from 5 μgC to 0.5 μgC and improves the accuracy of spectroscopic measurement methods to
125 0.2‰–0.3‰. The stable carbon isotope values of TC and WSOC in ambient PM_{2.5} were measured in
126 this study.

127 2.2 Bayesian stable isotope mixing model

128 The BSIM model could quantify the contributions of multiple sources to the TC and WSOC based on
129 the principle of mass conservation of stable isotopes, in which the Markov Chain Monte Carlo (MCMC)
130 method was employed. The methodology employed in the BSIM model was detailed in works by
131 Parnell et al. (2013) and Parnell and Inger (2010) (Parnell et al., 2010; Parnell et al., 2013). In brief, the

Deleted: The organic carbon (OC) and elemental carbon (EC) in PM_{2.5} were analyzed using an OC/EC analyzer (2001A, Desert Research Institute, Reno, Nevada, USA) following the IMPROVE A procedure.

136 posterior distribution for the Bayesian neural network (BNN) was calculated utilizing the prior
137 distribution and likelihood function based on Bayes theorem. Implementation of the BSIM model in
138 this study utilized the SIMMR package in R software ([https://cran.r-project.org/
139 web/packages/simmr/index.html](https://cran.r-project.org/web/packages/simmr/index.html)). Gelman diagnostic values, ranging from 1 to 1.01, all met the
140 criteria of the posterior prediction test, indicating robust model performance and reliable results.
141 Additionally, an uncertainty index (UI_{90}) was employed here to further characterize the uncertainty
142 strength of TC and WSOC source apportionments based on their posterior distribution. This index
143 refers to the difference between the proportional contributions of the maximum and minimum values in
144 the rapid increase segment divided by 90 with a 90 % cumulative probability ($UI_{90} = (PC_{95} - PC_5)/90$)
145 (Zaryab et al., 2022; Ji et al., 2017).

146 2.3 Stable carbon isotope spectrum of PM_{2.5} sources

147 The BSIM model requires the input of potential sources for carbonaceous aerosols, along with their
148 local source-specific stable carbon isotope values (fingerprints). In this study, we firstly employed the
149 PMF model to identify the potential sources of TC and WSOC (Text S1), with the aim of reducing the
150 uncertainty of the subsequent BSIM model and verifying the reliability of the BSIM results. The PMF
151 results showed that traffic emissions, SOA, and biomass burning are the major contributors to
152 carbonaceous aerosols in Shenzhen, which were similar to the previous results in Guangzhou (Huang et
153 al., 2014). In addition, a literature review indicated that secondary conversion sources could be further
154 subdivided into fresh SOC for the low oxidation state and aged SOC for the high oxidation state (Chen
155 et al., 2019; Presto et al., 2009; Mahrt et al., 2022; Shen et al., 2017). Ultimately, traffic emissions,
156 fresh SOC, aged SOC, and biomass burning (BB) were identified as the four potential sources of TC
157 and WSOC for BSIM model in this study. Since the PMF model lacks the mass spectral information of

Deleted: end-members

Deleted: The PMF model was employed to identify the TC sources based on PM_{2.5} chemical species concentrations (carbon components, water-soluble inorganic ions, elements, Text S1), and found traffic sources, secondary transformation sources, and biomass combustion sources as the major

Deleted: are

Deleted: S

Deleted: in Shenzhen

167 offline PM_{2.5} samples, it fails to distinguish between fresh SOC and aged SOC in TC, making it
168 challenging to investigate the water solubility characteristics of the SOC based on PMF results. BSIM
169 model simultaneously quantified of fresh and aged SOC separately in both TC and WSOC, thereby
170 enabling an estimation of SOC water solubility. This capability is used for the final analysis in this
171 study.

172 Recognizing the regional variability in stable carbon isotope fingerprints of PM_{2.5} sources (Yao et
173 al., 2022), this work obtained representative and locally specific carbon isotope profiles for the four
174 sources in Shenzhen. The measured profiles of the four sources were used as prior information in the
175 BSIM model for the follow-up analyses. For the traffic emissions, we measured the stable carbon
176 isotope values of TC and WSOC in PM_{2.5} that were collected from the Mount Tanglang tunnel
177 (dominated by diesel vehicles) and the Jiuweiling tunnel (dominated by petrol vehicles) in Shenzhen.

178 Fresh SOC was simulated through petrol vehicle bench tests. The lowest stable carbon isotope values
179 for TC and WSOC from the simulated samples were chosen as the fresh SOC results. The oxygen-
180 carbon ratios (O/C) of fresh SOC samples in this study ranged from 0.51 to 0.62, indicating a low

181 oxidation state (Ding et al., 2012). Aged SOC samples were obtained by collecting ambient PM_{2.5}
182 samples at the National Ambient Air Background Monitoring Station (Mount Wuzhi site, Hainan,
183 China), primarily influenced by regional pollution transported by northern continental air masses.

184 These aged SOC samples exhibited a high O/C value of 0.98, suggesting their highly oxidized state
185 (Zhu et al., 2016). Biomass burning emissions were simulated and analyzed by burning pine wood in
186 the Laboratory of Biomass Burning Simulation at Peking University Shenzhen Graduate School (He et
187 al., 2010). Additional details about the sampling process are available in the Supplementary

188 Information (Text S2). Table 1 summarizes the stable carbon isotope fingerprints of the four sources

Moved (insertion) [1]

Deleted: .

Deleted: and t

Deleted: PM_{2.5}

Deleted: s

Moved up [1]: The lowest stable carbon isotope values for TC and WSOC from the simulated sample were chosen as the fresh SOC results. Aged SOC samples were obtained by

Deleted: of SOA

Deleted: ambient PM_{2.5}

Deleted: values

199 and f_{60} signatures used in this study. Table S3 compares $\delta^{13}\text{C}_{\text{TC}}$ source signatures in this study with
 200 global datasets. The stable carbon isotope measurements from the four sources align with the range
 201 observed in global datasets, thus affirming the reliability of the four source fingerprints utilized in this
 202 study. Previous research identified $\text{C}_2\text{H}_4\text{O}_2^+$ (m/z 60) as a reliable marker for biomass burning in
 203 Shenzhen, with a feature value of 1.61 ± 0.68 % (Cao et al., 2018). This prior information was also
 204 incorporated into the BSIM model to estimate the biomass burning source. Although there is some
 205 overlap among the $\delta^{13}\text{C}$ fingerprints of different sources, the Bayesian approach allows for probabilistic
 206 estimation of the contribution of different sources and can also integrate information from multiple
 207 markers and sources to mitigate the effects of overlap. In this study, the PMF model was used to reduce
 208 the uncertainty of interference from unrelated sources, and the chemical tracer marker of biomass
 209 burning source (f_{60}) was also integrated to minimize the effect of this overlap.

Deleted: s, indicating that the measurement results fall within the range of global datasets.

210 **Table 1.** Stable carbon isotope fingerprints and f_{60} signatures for TC and WSOC sources.

Deleted: end-members

	Traffic		Fresh SOC		Aged SOC		BB	
	$\delta^{13}\text{C}/\text{‰}$	$f_{60}/\%$	$\delta^{13}\text{C}/\text{‰}$	$f_{60}/\%$	$\delta^{13}\text{C}/\text{‰}$	$f_{60}/\%$	$\delta^{13}\text{C}/\text{‰}$	$f_{60}/\%$
TC	-26.26 ± 0.50	0	-27.31 ± 0.73	0	-25.54 ± 0.28	0	-27.58 ± 0.24	1.61 ± 0.68
WSOC	Traffic		Fresh SOC		Aged SOC		BB	
	$\delta^{13}\text{C}/\text{‰}$	$f_{60}/\%$	$\delta^{13}\text{C}/\text{‰}$	$f_{60}/\%$	$\delta^{13}\text{C}/\text{‰}$	$f_{60}/\%$	$\delta^{13}\text{C}/\text{‰}$	$f_{60}/\%$
	-26.68 ± 0.37	0	-26.18 ± 0.75	0	-24.93 ± 0.39	0	-26.78 ± 0.17	1.61 ± 0.68

211 **2.4 Contributions of SOC to WIOC**

212 Based on the source apportionment results from the BSIM model for TC and WSOC, the contributions
 213 of fresh SOC and aged SOC to WIOC were calculated according to the equations (1-2). The
 214 uncertainties (u) in concentrations of Fresh SOC (WIOC) and Aged SOC (WIOC) were assessed using the
 215 uncertainty transfer equations (3-4). Fresh SOC and aged SOC uncertainties in both TC (14.9 %,
 216 30.1 %) and WSOC (24.1 %, 20.9 %) were determined using the BSIM model. Our findings reveal that

220 the calculated uncertainties of [Fresh SOC_(wIOC)] and [Aged SOC_(wIOC)] were 28.3 % and 36.8 %,
221 respectively.

$$222 \quad [\text{Fresh SOC}_{(wIOC)}] = [\text{Fresh SOC}_{(TC)}] - [\text{Fresh SOC}_{(WSOC)}] \quad (1)$$

$$223 \quad [\text{Aged SOC}_{(wIOC)}] = [\text{Aged SOC}_{(TC)}] - [\text{Aged SOC}_{(WSOC)}] \quad (2)$$

$$224 \quad u_{[\text{Fresh SOC}_{(wIOC)}]} = \left(u_{[\text{Fresh SOC}_{(TC)}]}^2 + u_{[\text{Fresh SOC}_{(WSOC)}]}^2 \right)^{1/2} \quad (3)$$

$$225 \quad u_{[\text{Aged SOC}_{(wIOC)}]} = \left(u_{[\text{Aged SOC}_{(TC)}]}^2 + u_{[\text{Aged SOC}_{(WSOC)}]}^2 \right)^{1/2} \quad (4)$$

226 3. Results and discussion

227 3.1 Overview of PM_{2.5} and carbonaceous components

228 The annual mean concentration of PM_{2.5} in Shenzhen was 24.9 µg/m³ in 2019, with TC being the
229 predominant component, exhibiting an annual mean concentration of 7.1 µg/m³ (5.8 and 1.3 µg/m³ for
230 OC and EC, respectively). WSOC accounts for 48 % of OC, presenting an annual mean concentration
231 of 2.8 µg/m³. The mean stable carbon isotope values for TC (δ¹³C_{TC}) and WSOC (δ¹³C_{WSOC}) were -
232 26.64 ± 0.79 ‰ and -25.80 ± 0.88 ‰, respectively, which is lower than the results of northern cities in
233 China (Wu et al., 2020). This can be attributed to the limited impact of coal combustion (which has
234 high ¹³C values) on PM_{2.5} in Shenzhen (Yao et al., 2022; Vodicka et al., 2022).

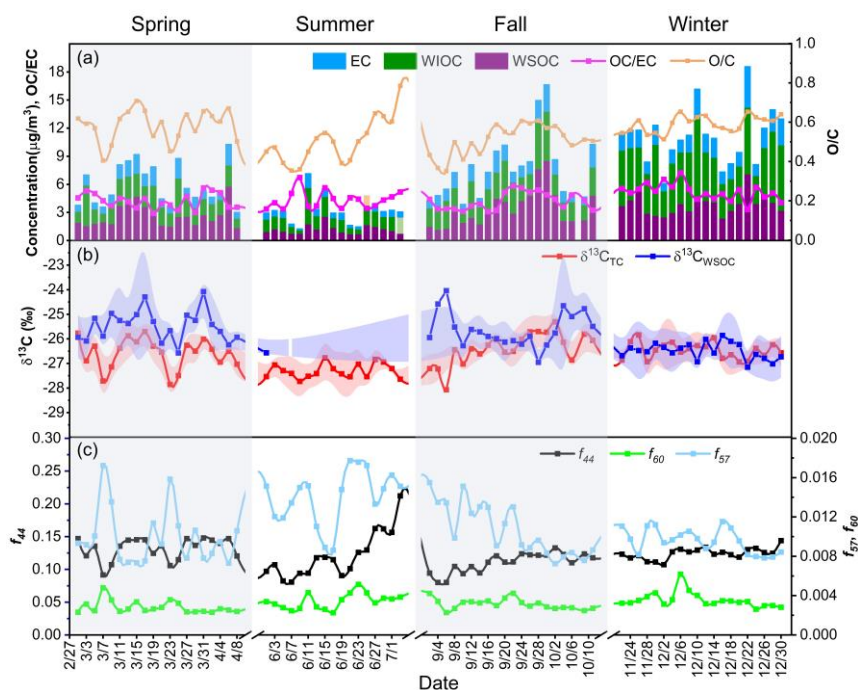
235 Seasonal variation revealed that TC, OC, WSOC, and EC exhibited elevated levels in winter and
236 decreased levels in summer (Fig. 2a). This pattern primarily stems from pollution air masses
237 originating from continental regions in the fall and winter, and clean air masses from the southern
238 ocean during the summer months (Fig. S1). The OC to EC ratio, averaging 4.5, was also higher in
239 winter than in summer, consistent with the Oxygen-to-Carbon (O/C) ratio results for WSOC (Fig. 2a),

240 indicating a large influence of aged SOC on carbonaceous aerosols in winter. The stable carbon isotope
241 results support this observation. Fig. 2b depicts relatively higher $\delta^{13}\text{C}_{\text{TC}}$ and $\delta^{13}\text{C}_{\text{WSOC}}$ values in spring
242 (-26.59‰, -25.26‰), fall (-26.38‰, -25.44‰), and winter (-26.46‰, -26.27‰). These higher values
243 are attributed to greater contributions of aged SOC from northern and northeast regional transport
244 processes during these seasons (Fig. S1). In summer, observed low $\delta^{13}\text{C}_{\text{TC}}$ and $\delta^{13}\text{C}_{\text{WSOC}}$ values of -
245 27.29‰ and -26.57‰, respectively, suggest relatively high contributions of fresh SOC to $\text{PM}_{2.5}$.
246 Shenzhen experiences high temperatures in summer, leading to increased gaseous precursor emissions
247 from terrestrial biogenic sources, especially C3 plants. Intense solar radiation and high temperature
248 favor photochemical reactions to generate fresh SOC that depletes ^{13}C in particulate matter during
249 summer (Kirillova et al., 2013).

250 Mass spectra characteristics of CO_2^+ (m/z 44), C_4H_9^+ (m/z 57), and $\text{C}_2\text{H}_4\text{O}_2^+$ (m/z 60) in WSOC
251 were measured to represent oxidized organic aerosol (OOA), hydrocarbon-like organic Aerosol (HOA),
252 and biomass burning organic aerosol (BBOA), respectively. The abundance of these ion fragments,
253 denoted as f_{44} , f_{57} , and f_{60} , is determined by the ratios of signal intensities at m/z 44, m/z 57, and m/z 60
254 to the sum of signal intensities from all m/z signals in the organic mass spectra. As depicted in Fig. 2c,
255 f_{44} obtained higher values in spring (0.131) and winter (0.125) compared to summer (0.120) and fall
256 (0.112), further indicating an elevated oxidation level of OOA during spring and winter. Considering
257 that f_{60} exceeds 0.0030 when biomass burning influences carbonaceous aerosol (Docherty et al., 2008;
258 DeCarlo et al., 2008), the annual average value of f_{60} was 0.0032, suggesting biomass burning was an
259 important source of carbon components in Shenzhen. Winter exhibited higher levels of f_{60} (0.0035)
260 compared to other seasons, suggesting relatively strong impacts of biomass burning on WSOC in
261 winter. Conversely, f_{57} reached its highest level in summer (0.014) and the lowest in winter (0.009),

Deleted: ure

263 with an annual average value of 0.011, possibly associated with a notable increase in hydrocarbon
 264 organic aerosol emissions from traffic and biogenic sources during the summer period.

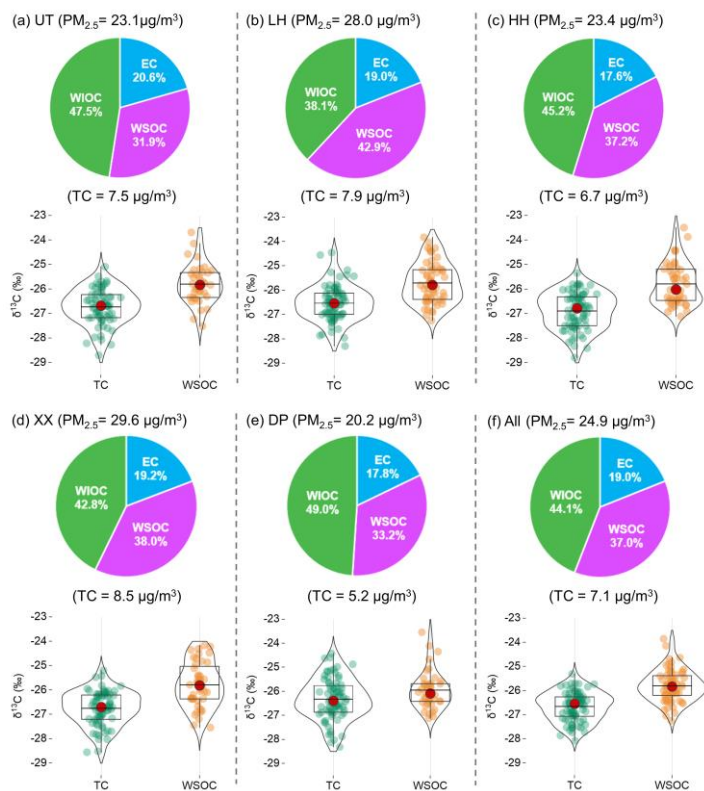


265
 266 **Figure 2.** Time series of carbonaceous components (a), stable carbon isotope characteristics of TC and
 267 WSOC(b), and mass spectra signatures of WSOC in $\text{PM}_{2.5}$ (c) from Shenzhen. Each data was averaged
 268 from five sampling sites. (Note: Summer samples exhibit elevated analytical errors due to low
 269 concentrations, and $\delta^{13}\text{C}_{\text{WSOC}}$ values are computed from combined summer samples).

270 Obvious spatial variations in $\text{PM}_{2.5}$ mass concentrations across Shenzhen during 2019 were
 271 observed, with XX site registering the highest concentration ($29.6 \mu\text{g}/\text{m}^3$), followed by LH (28.0
 272 $\mu\text{g}/\text{m}^3$), HH ($23.4 \mu\text{g}/\text{m}^3$), UT ($23.1 \mu\text{g}/\text{m}^3$), and DP ($20.2 \mu\text{g}/\text{m}^3$). Fig. 3 illustrates that TC made more
 273 substantial contributions ($28.2\% \sim 32.5\%$) to $\text{PM}_{2.5}$ at the four urban sites in the central and western
 274 regions of Shenzhen compared to the background site (DP, 25.7%). This suggests that local pollutant

Deleted: ure

276 emissions significantly influence carbonaceous aerosols in Shenzhen's urban areas. The percentage of
277 WSOC in TC was also higher in urban areas (37.5 ± 3.9 %) compared to the background area (DP,
278 33.2 %), reaching the highest value at the LH site (42.9 %). However, the percentage of WIOC in TC
279 displayed the opposite trend, suggesting carbonaceous aerosols in urban areas of Shenzhen exhibit
280 higher water solubility than in background areas. Distinct spatial distribution characteristics were also
281 observed in the stable carbon isotopes of TC and WSOC. The background site exhibits higher $\delta^{13}\text{C}_{\text{TC}}$
282 values (-26.33 %) than the four urban sites (-26.72 ± 0.13 %). This difference may be attributed to the
283 increased contribution of traffic or fresh SOC sources to carbonaceous aerosols at urban sites and the
284 relatively high contribution of aged SOC at the background site. Atmospheric aging processes of
285 organics through photochemical reactions can deplete ^{13}C in aged SOC and enrich ^{13}C in fresh SOC
286 and other related reactants simultaneously (Pavuluri and Kawamura 2017). While the close proximity
287 of the $\delta^{13}\text{C}_{\text{WSOC}}$ values at urban sites (-25.77 ± 0.04 ‰) to the background site (DP, -25.96 ‰) suggests
288 that the WSOC in different areas of Shenzhen may share a similar origin.



289

290 **Figure 3.** Chemical compositions of TC, $\delta^{13}\text{C}_{\text{TC}}$, and $\delta^{13}\text{C}_{\text{WSOC}}$ in $\text{PM}_{2.5}$ at urban sites (a-d), background
 291 site (e), and average result from all five sites (f). The Violin Box-and-Line Plots on the right display
 292 spatial variations of $\delta^{13}\text{C}_{\text{TC}}$ and $\delta^{13}\text{C}_{\text{WSOC}}$ at each site, featuring mean values (black lines) and median
 293 values (red dots).

294 3.2 Source apportionment results for TC and WSOC

295 The BSIM model assessed the contributions of traffic source, fresh SOC, aged SOC, and biomass
 296 burning (BB) to TC and WSOC, as shown in Fig. 4. On average, SOC (total of fresh and aged SOC)
 297 and traffic emerged as the two major contributors to TC, accounting for 43 % and 40 % respectively,
 298 while biomass burning contributed 17 % to TC. The contribution of aged SOC to TC (23 %) is
 299 comparable with fresh SOC (20 %). Regarding WSOC, SOC was the dominant source, comprising 45 %

300 of aged SOC and 28 % of fresh SOC, followed by BB (18 %) and Traffic (9 %). The noteworthy
301 contribution of aged SOC to WSOC suggests a comparatively higher water solubility of aged SOC in
302 Shenzhen.

303 To evaluate the BSIM model's performance, we employed the PMF model to apportion the
304 sources of TC and WSOC. The obtained results were subsequently compared with those from the
305 BSIM model, as depicted in Fig. 4a. Seventeen chemical species of PM_{2.5} were applied as the PMF
306 model input to estimate source contributions to TC, encompassing carbon components, soluble
307 inorganic ions, and elements. For the apportionment of WSOC sources, five species including WSOC,
308 WIOC, and three organic mass spectra were applied as the PMF model input. More details about the
309 PMF model and results can be found in the Supplementary Information (Text S1, Fig. S2-S5). PMF
310 identified the traffic as the predominant contributor to TC (55 %), followed by SOC (34 %) and
311 biomass burning (4 %). Concerning WSOC, aged SOC and fresh SOC were the two major sources as
312 well, accounting for 43 % and 27 %, respectively. The traffic contribution to TC apportioned by the
313 PMF model is higher than that of the BSIM model (55 % vs. 40 %), which may be due to the fact that
314 some of the fresh SOC generated by the conversion of primary vehicle emissions was improperly
315 apportioned to the traffic source in the PMF model (Li et al., 2022; Zhao et al., 2014). Previous study
316 also showed that SOA contributes more to carbonaceous aerosols in Shenzhen than the traffic source
317 (Cao et al., 2022). The PMF model results for WSOC were generally consistent with BSIM model
318 results, with deviations primarily attributed to the differences in the principles and uncertainties of the
319 two models.

320 Furthermore, this study examined cumulative frequency distributions to elucidate the inherent

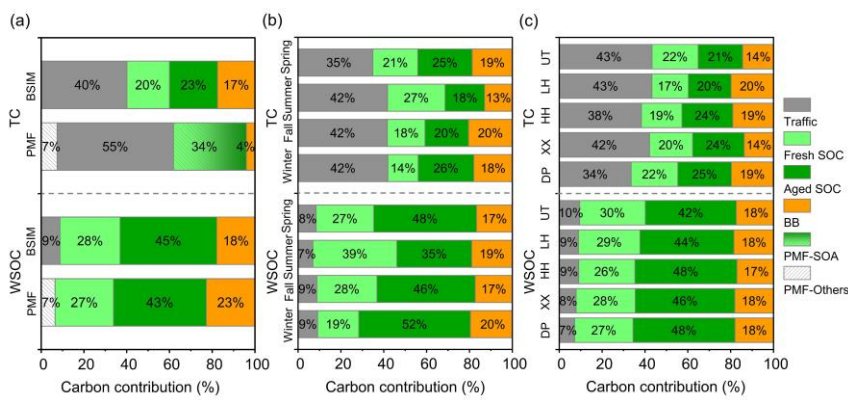
Deleted: 4

Deleted: S

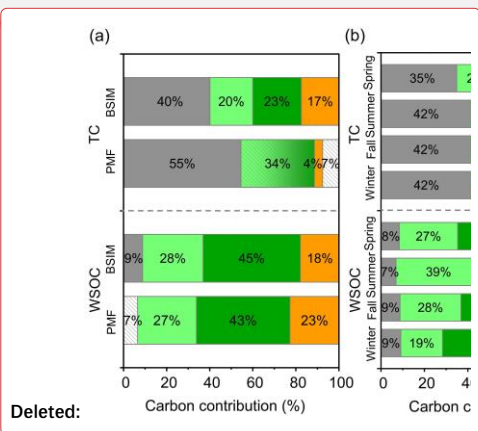
322 uncertainty in source apportionments of TC and WSOC. As shown in Fig. 5a and b, the proportional
323 contributions of BB source to both TC and WSOC were quite stable during the research periods due to
324 its low UI_{90} value (0.02). This may be attributed to the incorporation of mass spectral constraints for
325 the BB source in the BSIM model used in this study. For TC source apportionment results, the largest
326 UI_{90} value (0.46) was observed for the traffic source, indicating that its contribution to TC exhibited
327 relatively high uncertainty. In 90 % probability, its contribution ranged from 19.4 % to 60.9 %. The
328 UI_{90} values for fresh and aged SOC were 0.15 and 0.30, respectively. Regarding WSOC, the calculated
329 UI_{90} value of traffic, fresh SOC, and aged SOC ranged from 0.18 to 0.24. The UI_{90} values obtained
330 through the BSIM model remained within reasonable limits, and were smaller than those calculated in
331 previous related studies (0.23-0.62) (Zaryab et al., 2022; Ji et al., 2017). Consequently, the source
332 contributions of TC and WSOC estimated by the BSIM model in this study were deemed reasonable.

333 For seasonal variations, as shown in Fig. 4b, SOC still was the major source of TC and WSOC
334 during all four seasons, ranging from 38 % ~ 46 % and 71 % ~ 75 % respectively. Significant high
335 contributions of fresh SOC to TC and WSOC occurred in summer (27 %, 39 %), and relatively higher
336 contributions of aged SOC to TC and WSOC were observed in winter (26 %, 52 %). It is because
337 meteorological conditions in winter characterized by inversions and stagnant winds facilitate the
338 accumulation of air pollutants, and Shenzhen is largely influenced by regional pollution transport in
339 winter, favoring the formation of aged SOC (Huang et al., 2018). In contrast, favorable meteorological
340 conditions (e.g. intense and prolonged solar radiation, high temperatures, and relative humidity) in
341 summer enhanced photochemical reactions to generate fresh SOC. In terms of spatial distributions (Fig.
342 4c), the contributions of the traffic source to TC were higher at urban sites (38 % to 43 %) compared to
343 the background site (34 %). This finding aligns with expectations due to increased human activity and

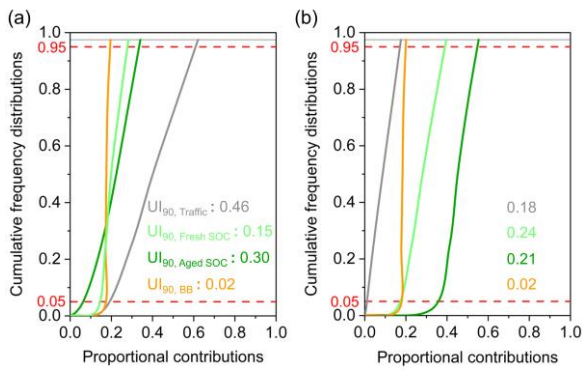
345 vehicle numbers in urban locations. At the DP site, the contributions of SOC to TC were higher than
 346 those of other sources (47 %), signifying a predominant influence of regionally transported pollutant
 347 emissions on TC at the background site. However, the contributions of SOC and the other two primary
 348 sources at both urban and background sites were all close to each other, indicating the source
 349 composition of WSOC in Shenzhen is less affected by air pollution degree compared to TC.



350



351 **Figure 4.** (a) Comparison of source apportionment results between BSIM model and PMF model for
 352 TC and WSOC, (b) seasonal and (c) spatial distributions of source apportionment results for TC and
 353 WSOC based on the BSIM model.



354

355 **Figure 5.** Cumulative frequency distributions of the proportional contributions from potential sources
 356 of TC (a) and WSOC (b) based on BSIM model.

358 3.3 Water solubility of fresh SOC and aged SOC

359 The contributions of fresh SOC and aged SOC to WIOC were the differences between the contributions
360 of those two SOC sources to TC and WSOC from the BSIM model (Sect. 2.4) in this study. As shown
361 in Fig. 6a, fresh SOC and aged SOC made contributions of $23.2\pm 4.2\%$ and $13.4\pm 3.8\%$ to WIOC,
362 respectively, implying that primary sources are the dominant contributors to WIOC. Further support for
363 this finding is evident in the strong correlation between WIOC and EC, as depicted in Fig. 6b. A higher
364 slope was observed in winter (2.4) than in other seasons, consistent with the highest contributions of
365 aged SOC to WIOC in winter (22 %). This observation implies that WIOC in winter is influenced not
366 only by local primary sources but also by the promotion of secondary pollution.

367 To investigate deeply the water solubility characteristics of fresh and aged SOC, we then calculate
368 their water-soluble fraction by comparing their water-soluble portion to the ambient fraction ($[c]_{\text{water-}}$
369 $\text{soluble}/([c]_{\text{water-soluble}} + [c]_{\text{water-insoluble}})$, where $[c]_{\text{water-soluble}}$ and $[c]_{\text{water-insoluble}}$ are the concentrations of fresh
370 SOC or aged SOC in WSOC and WIOC, respectively) (Li et al., 2021). As shown in Fig. 6c, the overall
371 water-soluble fraction of SOC in this study was 66.2 % with a range from 58.9 % to 76.0 %. Fresh
372 SOC exhibited a much lower water-solubility of 54.2 %, whereas aged SOC displayed a comparatively
373 higher water-solubility of 76.5 %. The higher water solubility of aged SOC compared to fresh SOC
374 might be due to the positive correlation between aerosol hygroscopicity and oxidation in the sub-
375 saturated state. The water-soluble fraction of SOC in this study was close to that reported in other
376 coastal cities (Tokyo (71 %) and Southeastern United States (60 %)) (Kondo et al., 2007; Verma et al.,
377 2015), while was much higher than that reported in northern Chinese cities (Beijing (42 % ~ 45 %) and
378 Handan (49 %)) (Li et al., 2021; Qiu et al., 2019). In addition, the water-soluble fraction of both fresh
379 SOC and aged SOC, as calculated in this study, was comparable to that reported in Guangzhou (61 %

Deleted: 5

Deleted: 5

Deleted: and c

Deleted: WIOC/EC ratio

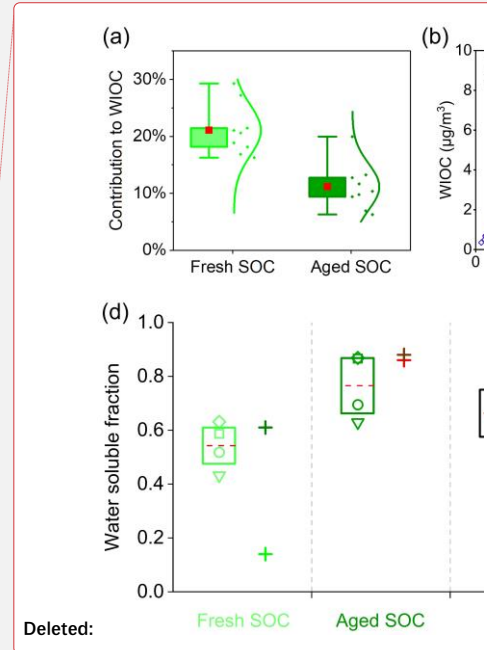
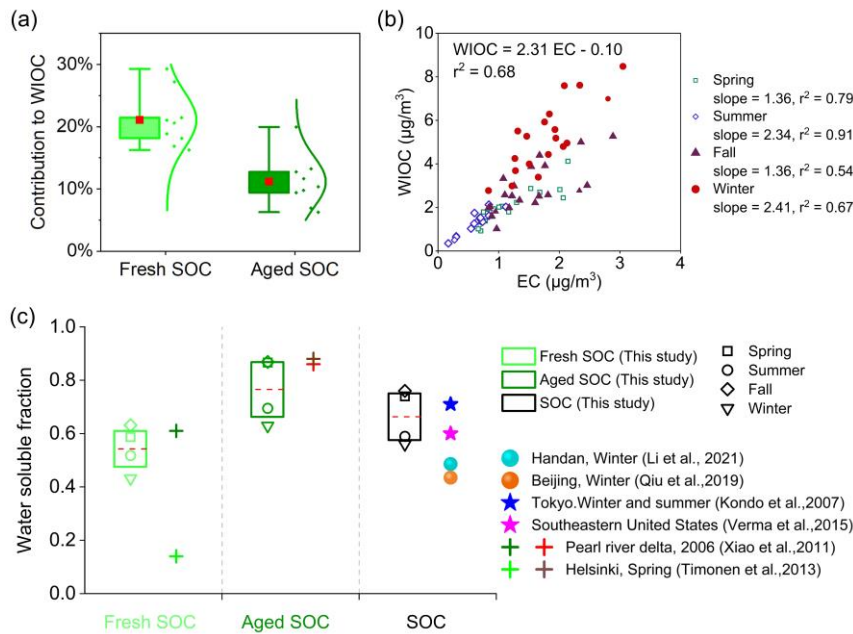
Deleted: 9

Deleted: 5

Deleted: d

387 and 86 % for fresh and aged SOC respectively) (Xiao et al., 2011). This could be attributed to
388 Shenzhen's coastal location, which is markedly influenced by regional transport from neighboring
389 urban areas and the eastern seaboard air masses. The high relative humidity facilitates the conversion of
390 aged SOC into WSOC during the pollution transport process. This result is in accordance with previous
391 findings that air masses influenced by anthropogenic emissions could promote the formation of high
392 water-soluble SOA under high relative humidity in urban environments (Miyazaki et al., 2006; Salma
393 et al., 2007; Weber et al., 2007). Given that the aging process of SOA dissolved in water could enhance
394 the cloud condensation nuclei (CCN) activity of the particles (Liu and Matsui 2022), high water-
395 soluble aged SOC in Shenzhen might have significant impacts on the activity of CCN, potentially
396 resulting in more important indirect climate effects.

397 The water-soluble fraction of SOC (especially aged SOC) in Shenzhen exhibits obvious seasonal
398 characteristics, with the highest in fall (76.0 %) and the lowest in winter (56.0 %). This phenomenon is
399 primary related to the robust atmospheric oxidizing capacity during fall in Shenzhen since the
400 atmospheric oxidants such as OH and NO₃ radicals play pivotal roles in driving the secondary
401 generation of WSOC (Wang et al., 2023). Conversely, during winter, the temperature and relative
402 humidity are at their lowest levels, and the relatively diminished atmospheric oxidizing capacity also
403 constrains the secondary generation of WSOC.



404

405 **Figure 6.** (a) Left is the box and whisker plots of fresh and aged SOC contributions to WIOC, the
 406 upper and lower of the box representing the 75th and 25th percentiles, and the red squares featuring
 407 mean values. The dots on the right show the contribution of fresh and aged SOC to WIOC across
 408 seasons and sites, the curve demonstrates its normal distribution. (b) Scatterplot of WIOC versus EC by
 409 season. (c) Comparison of the water-soluble fraction of SOC (fresh SOC, aged SOC, SOC) in this
 410 study (box and whisker plots) with those in other related literature (colored markings on the right). The
 411 upper and lower of the box represent the 75th and 25th percentiles and the dashed red lines indicate
 412 mean values.

413 **4. Summary and implications**

414 Assessing the impacts of different oxidational SOC on air quality and its water solubility has been
 415 challenging, and this work successfully evaluated the water-soluble fraction of fresh and aged SOC
 416 employing the BSIM model on one-year observational data for stable carbon isotopes and mass spectra
 417 of TC and WSOC in Shenzhen, China. Compared with other methods, e.g. PMF model, EC tracer, and

Deleted: 5
 Deleted: B

Deleted: .
 Deleted: . (c) Seasonal variation of WIOC/EC ratio
 Deleted: d

Deleted: (Kondo et al., 2007; Li et al., 2021; Qiu et al., 2019; Timonen et al., 2013; Verma et al., 2015; Xiao et al., 2011)...

426 multiple linear regression analyses, the BSIM model successfully calculated the contributions of fresh
427 SOC and aged SOC to WSOC and WIOC, owing to prior and localized information about stable carbon
428 isotopes and mass spectra of PM_{2.5} sources. Therefore, establishing localized carbonaceous aerosol
429 source profiles for stable carbon isotopes becomes crucial for comprehending the relationship between
430 the aging degree and water solubility of SOC.

431 The observed average mass concentration of PM_{2.5} during the sampling period in Shenzhen was
432 24.9 µg/m³, and WSOC accounts for 48 % of OC. The mean stable carbon isotope values for TC
433 ($\delta^{13}\text{C}_{\text{TC}}$) and WSOC ($\delta^{13}\text{C}_{\text{WSOC}}$) were $-26.64 \pm 0.79 \text{ ‰}$ and $-25.80 \pm 0.88 \text{ ‰}$, respectively. WSOC was
434 dominated by secondary sources while WIOC was dominated by primary sources. The contribution of
435 fresh SOC and aged SOC to WSOC, WIOC were 28.1 % and 45.2 %, 23.2 % and 13.4 %, respectively.
436 The overall water-soluble fraction of SOC in this study was 66.2 %, with aged SOC constituting 76.5 %
437 and fresh SOC 54.2 %. The water-soluble fraction of aged SOC was 22 % higher than fresh SOC, even
438 though both of them demonstrated remarkable water-soluble characteristics in Shenzhen. This finding
439 highlights the important role of aged SOC in the water uptake process of particulate matter.
440 Considering the strong correlation between the water solubility of SOC and its light extinction effect,
441 further exploration of the extinction effect of SOC with different aging degrees will greatly contribute
442 to a more profound understanding of the extinction mechanism of SOC. Besides, the water solubility of
443 SOC in coastal cities was observed to be higher than that in inland cities, suggesting a more
444 pronounced climate effect of SOC in coastal cities. Therefore, there should be increased emphasis on
445 enhancing the control of SOA precursors in coastal urban areas to better integrate air pollution and
446 climate change management. This is particularly crucial given the observed rise in the proportion of
447 SOA in particulate matter in recent years. Moreover, the results of our study further hinted that the

448 notable water solubility of SOC, particularly aged SOC, may contribute a lot to the formation of CCN
449 above coastal cities, which is also helpful to a better understanding of the cloud microphysical
450 processes and the indirect climate effect of SOC in coastal urban regions.

451 **Data availability.** Datasets are available by contacting the corresponding author, Xing Peng
452 (pengxing@pku.edu.cn)

453

454 **Author contributions.** PX and HX conceptualized the study. WF, CL, TM and FN retrieved and
455 constructed the dataset. WF and PX carried out the statistical analysis. WF prepared the first draft of
456 the manuscript, which was commented on and revised by PX, HL, and HX. All authors reviewed and
457 approved the final version for publication.

458

459 **Competing interests.** The authors declare that they have no conflict of interest.

460

461 **Financial support.** This research has been supported by the National Key Research and Development
462 Program of China (2023YFC3709203) and the Science and Technology Plan of Shenzhen Municipality
463 (JCYJ20220818100812028).

464 **References**

- 465 Cao, L. M., Huang, X. F., Li, Y. Y., Hu, M. & He, L. Y. (2018) Volatility measurement of
466 atmospheric submicron aerosols in an urban atmosphere in southern China. *Atmos. Chem.*
467 *Phys.*, 18, 1729-1743.
- 468 Cao, L. M., Wei, J., He, L. Y., Zeng, H., Li, M. L., Zhu, Q., Yu, G. H. & Huang, X. F. (2022)
469 Aqueous aging of secondary organic aerosol coating onto black carbon: Insights from
470 simultaneous L-ToF-AMS and SP-AMS measurements at an urban site in southern China. *J.*
471 *Clean. Prod.*, 330.
- 472 Ceburnis, D., Garbaras, A., Szidat, S., Rinaldi, M., Fahrni, S., Perron, N., Wacker, L., Leinert, S.,
473 Remeikis, V., Facchini, M. C., Prevot, A. S. H., Jennings, S. G., Ramonet, M. & O'Dowd, C.
474 D. (2011) Quantification of the carbonaceous matter origin in submicron marine aerosol by
475 ^{13}C and ^{14}C isotope analysis. *Atmos. Chem. Phys.*, 11, 8593-8606.
- 476 Chen, T., Liu, Y., Chu, B., Liu, C., Liu, J., Ge, Y., Ma, Q., Ma, J. & He, H. (2019) Differences of
477 the oxidation process and secondary organic aerosol formation at low and high precursor
478 concentrations. *J Environ Sci (China)*. 79, 256-263.
- 479 DeCarlo, P. F., Dunlea, E. J., Kimmel, J. R., Aiken, A. C., Sueper, D., Crouse, J., Wennberg, P. O.,
480 Emmons, L., Shinozuka, Y., Clarke, A., Zhou, J., Tomlinson, J., Collins, D. R., Knapp, D.,
481 Weinheimer, A. J., Montzka, D. D., Campos, T. & Jimenez, J. L. (2008) Fast airborne aerosol
482 size and chemistry measurements above Mexico City and Central Mexico during the
483 MILAGRO campaign. *Atmos. Chem. Phys.*, 8, 4027-4048.
- 484 Ding, X., Wang, X. M., Gao, B., Fu, X. X., He, Q. F., Zhao, X. Y., Yu, J. Z. & Zheng, M. (2012)
485 Tracer-based estimation of secondary organic carbon in the Pearl River Delta, south China. *J.*

486 *Geophys. Res. Atmos.*, 117, 1-14.

487 Docherty, K. S., Stone, E. A., Ulbrich, I. M., DeCarlo, P. F., Snyder, D. C., Schauer, J. J., Peltier, R.
488 E., Weber, R. J., Murphy, S. M., Seinfeld, J. H., Grover, B. D., Eatough, D. J. & Jimenez, J. L.
489 (2008) Apportionment of primary and secondary organic aerosols in Southern California
490 during the 2005 study of organic aerosols in riverside (SOAR-1). *Environ. Sci. Technol.*, 42,
491 7655-7662.

492 Donaldson, D. J. & George, C. (2012) Sea-surface chemistry and its impact on the marine
493 boundary layer. *Environ. Sci. Technol.*, 46, 10385-10389.

494 Favez, O., Sciare, J., Cachier, H., Alfaro, S. C. & Abdelwahab, M. M. (2008) Significant
495 formation of water-insoluble secondary organic aerosols in semi-arid urban environment.
496 *Geophys. Res. Lett.*, 35.

497 Fushimi, A., Wagai, R., Uchida, M., Hasegawa, S., Takahashi, K., Kondo, M., Hirabayashi, M.,
498 Morino, Y., Shibata, Y., Ohara, T., Kobayashi, S. & Tanabe, K. (2011) Radiocarbon (¹⁴C)
499 diurnal variations in fine particles at sites downwind from Tokyo, Japan in summer. *Environ.*
500 *Sci. Technol.*, 45, 6784-92.

501 Han, S., Hong, J., Luo, Q., Xu, H., Tan, H., Wang, Q., Tao, J., Zhou, Y., Peng, L., He, Y., Shi, J.,
502 Ma, N., Cheng, Y. & Su, H. (2022) Hygroscopicity of organic compounds as a function of
503 organic functionality, water solubility, molecular weight, and oxidation level. *Atmos. Chem.*
504 *Phys.*, 22, 3985-4004.

505 He, L. Y., Lin, Y., Huang, X. F., Guo, S., Xue, L., Su, Q., Hu, M., Luan, S. J. & Zhang, Y. H. (2010)
506 Characterization of high-resolution aerosol mass spectra of primary organic aerosol
507 emissions from Chinese cooking and biomass burning. *Atmos. Chem. Phys.*, 10, 11535-11543.

508 Huang, R. J., Zhang, Y., Bozzetti, C., Ho, K. F., Cao, J. J., Han, Y., Daellenbach, K. R., Slowik, J.
509 G., Platt, S. M., Canonaco, F., Zotter, P., Wolf, R., Pieber, S. M., Bruns, E. A., Crippa, M.,
510 Ciarelli, G., Piazzalunga, A., Schwikowski, M., Abbaszade, G., Schnelle-Kreis, J.,
511 Zimmermann, R., An, Z., Szidat, S., Baltensperger, U., El Haddad, I. & Prevot, A. S. (2014)
512 High secondary aerosol contribution to particulate pollution during haze events in China.
513 *Nature.*, 514, 218-22.

514 Huang, X. F., Zou, B. B., He, L. Y., Hu, M., Prévôt, A. S. H. & Zhang, Y. H. (2018) Exploration of
515 PM_{2.5} sources on the regional scale in the Pearl River Delta based on ME-2 modeling. *Atmos.*
516 *Chem. Phys.*, 18, 11563-11580.

517 Ji, X. L., Xie, R. T., Hao, Y. & Lu, J. (2017) Quantitative identification of nitrate pollution sources
518 and uncertainty analysis based on dual isotope approach in an agricultural watershed. *Environ.*
519 *Pollut.*, 229, 586-594.

520 Jiang, F., Liu, J., Cheng, Z., Ding, P., Xu, Y., Zong, Z., Zhu, S., Zhou, S., Yan, C., Zhang, Z.,
521 Zheng, J., Tian, C., Li, J. & Zhang, G. (2022) Dual-carbon isotope constraints on source
522 apportionment of black carbon in the megacity Guangzhou of the Pearl River Delta region,
523 China for 2018 autumn season. *Environ. Pollut.*, 294, 118638.

524 Kaul, D. S., Gupta, T., Tripathi, S. N., Tare, V. & Collett, J. L. (2011) Secondary organic aerosol: a
525 comparison between foggy and nonfoggy days. *Environ. Sci. Technol.*, 45, 7307-7313.

526 Kirillova, E. N., Andersson, A., Sheesley, R. J., Kruså, M., Praveen, P. S., Budhavant, K., Safai, P.
527 D., Rao, P. S. P. & Gustafsson, Ö. (2013) ¹³C- and ¹⁴C-based study of sources and
528 atmospheric processing of water-soluble organic carbon (WSOC) in South Asian aerosols. *J.*
529 *Geophys. Res. Atmos.*, 118, 614-626.

530 Kondo, Y., Miyazaki, Y., Takegawa, N., Miyakawa, T., Weber, R. J., Jimenez, J. L., Zhang, Q. &
531 Worsnop, D. R. (2007) Oxygenated and water-soluble organic aerosols in Tokyo. *J. Geophys.*
532 *Res. Atmos.*, 112.

533 Li, H., Zhang, Q., Jiang, W., Collier, S., Sun, Y., Zhang, Q. & He, K. (2021) Characteristics and
534 sources of water-soluble organic aerosol in a heavily polluted environment in Northern China.
535 *Sci. Total Environ.*, 758, 143970.

536 Li, S. Y., Liu, D. T., Kong, S. F., Wu, Y. Z., Hu, K., Zheng, H., Cheng, Y., Zheng, S. R., Jiang, X.
537 T., Ding, S., Hu, D. W., Liu, Q., Tian, P., Zhao, D. L. & Sheng, J. J. (2022) Evolution of
538 source attributed organic aerosols and gases in a megacity of central China. *Atmos. Chem.*
539 *Phys.*, 22, 6937-6951.

540 Lim, S., Hwang, J., Lee, M., Czimeczik, C. I., Xu, X. & Savarino, J. (2022) Robust Evidence of
541 14C, 13C, and 15N Analyses Indicating Fossil Fuel Sources for Total Carbon and
542 Ammonium in Fine Aerosols in Seoul Megacity. *Environ. Sci. Technol.*, 56, 6894-6904.

543 Liu, L., Kuang, Y., Zhai, M., Xue, B., He, Y., Tao, J., Luo, B., Xu, W., Tao, J., Yin, C., Li, F., Xu,
544 H., Deng, T., Deng, X., Tan, H. & Shao, M. (2022) Strong light scattering of highly
545 oxygenated organic aerosols impacts significantly on visibility degradation. *Atmos. Chem.*
546 *Phys.*, 22, 7713-7726.

547 Liu, M. X. & Matsui, H. (2022) Secondary organic aerosol formation regulates cloud
548 condensation nuclei in the global remote troposphere. *Geophys. Res. Lett.*, 49.

549 Mahrt, F., Peng, L., Zaks, J., Huang, Y., Ohno, P. E., Smith, N. R., Gregson, F. K. A., Qin, Y.,
550 Faiola, C. L., Martin, S. T., Nizkorodov, S. A., Ammann, M. & Bertram, A. K. (2022) Not all
551 types of secondary organic aerosol mix: two phases observed when mixing different

552 secondary organic aerosol types. *Atmos. Chem. Phys.*, 22, 13783-13796.

553 Miyazaki, Y., Kondo, Y., Takegawa, N., Komazaki, Y., Fukuda, M., Kawamura, K., Mochida, M.,
554 Okuzawa, K. & Weber, R. J. (2006) Time-resolved measurements of water-soluble organic
555 carbon in Tokyo. *J. Geophys. Res. Atmos.*, 111.

556 Parnell, A. C., Inger, R., Bearhop, S. & Jackson, A. L. (2010) Source partitioning using stable
557 isotopes: coping with too much variation. *PLoS One.*, 5, e9672.

558 Parnell, A. C., Phillips, D. L., Bearhop, S., Semmens, B. X., Ward, E. J., Moore, J. W., Jackson, A.
559 L., Grey, J., Kelly, D. J. & Inger, R. (2013) Bayesian stable isotope mixing models.
560 *Environmetrics.*, 24, 387-399.

561 Pavuluri, C. M. & Kawamura, K. (2017) Seasonal changes in TC and WSOC and their ¹³C
562 isotope ratios in Northeast Asian aerosols: land surface-biosphere-atmosphere interactions.
563 *Acta Geochimica*, 36, 355-358.

564 Plasencia Sánchez, E., Sánchez-Soberón, F., Rovira, J., Sierra, J., Schuhmacher, M., Soler, A.,
565 Torrentó, C. & Rosell, M. (2023) Integrating dual C and N isotopic approach to elemental
566 and mathematical solutions for improving the PM source apportionment in complex urban
567 and industrial cities: Case of Tarragona - Spain. *Atmos. Environ.*, 293.

568 Presto, A., Miracolo, M., Kroll, J., Worsnop, D., Robinson, A. & Donahue, N. (2009)
569 Intermediate-volatility organic compounds: a potential source of ambient oxidized organic
570 aerosol. *Environ. Sci. Technol.*, 43, 4744-4749.

571 Pye, H. O. T., Murphy, B. N., Xu, L., Ng, N. L., Carlton, A. G., Guo, H., Weber, R., Vasilakos, P.,
572 Appel, K. W., Budisulistiorini, S. H., Surratt, J. D., Nenes, A., Hu, W., Jimenez, J. L.,
573 Isaacman-VanWertz, G., Misztal, P. K. & Goldstein, A. H. (2017) On the implications of

574 aerosol liquid water and phase separation for organic aerosol mass. *Atmos. Chem. Phys.*, 17,
575 343-369.

576 Qiu, Y., Xie, Q., Wang, J., Xu, W., Li, L., Wang, Q., Zhao, J., Chen, Y., Chen, Y., Wu, Y., Du, W.,
577 Zhou, W., Lee, J., Zhao, C., Ge, X., Fu, P., Wang, Z., Worsnop, D. R. & Sun, Y. (2019)
578 Vertical characterization and source apportionment of water-soluble organic aerosol with
579 high-resolution aerosol mass spectrometry in Beijing, China. *ACS Earth Space Chem.*, 3,
580 273-284.

581 Salma, I., Ocskay, R., Chi, X. & Maenhaut, W. (2007) Sampling artefacts, concentration and
582 chemical composition of fine water-soluble organic carbon and humic-like substances in a
583 continental urban atmospheric environment. *Atmos. Environ.*, 41, 4106-4118.

584 Shen, Z., Zhang, Q., Cao, J., Zhang, L., Lei, Y., Huang, Y., Huang, R. J., Gao, J., Zhao, Z., Zhu, C.,
585 Yin, X., Zheng, C., Xu, H. & Liu, S. (2017) Optical properties and possible sources of brown
586 carbon in PM_{2.5} over Xi'an, China. *Atmos. Environ.*, 150, 322-330.

587 Shrivastava, M., Cappa, C. D., Fan, J. W., Goldstein, A. H., Guenther, A. B., Jimenez, J. L., Kuang,
588 C., Laskin, A., Martin, S. T., Ng, N. L., Petaja, T., Pierce, J. R., Rasch, P. J., Roldin, P.,
589 Seinfeld, J. H., Shilling, J., Smith, J. N., Thornton, J. A., Volkamer, R., Wang, J., Worsnop, D.
590 R., Zaveri, R. A., Zelenyuk, A. & Zhang, Q. (2017) Recent advances in understanding
591 secondary organic aerosol: Implications for global climate forcing. *Rev. Geophys.*, 55, 509-
592 559.

593 Tang, T., Cheng, Z., Xu, B., Zhang, B., Zhu, S., Cheng, H., Li, J., Chen, Y. & Zhang, G. (2020)
594 Triple Isotopes $\delta^{13}\text{C}$, $\delta^2\text{H}$, and $\delta^{14}\text{C}$ Compositions and Source Apportionment of
595 Atmospheric Naphthalene: A Key Surrogate of Intermediate-Volatility Organic Compounds

596 (IVOCs). *Environ. Sci. Technol.*, 54, 5409-5418.

597 Timonen, H., Carbone, S., Aurela, M., Saarnio, K., Saarikoski, S., Ng, N. L., Canagaratna, M. R.,
598 Kulmala, M., Kerminen, V.-M., Worsnop, D. R. & Hillamo, R. (2013) Characteristics,
599 sources and water-solubility of ambient submicron organic aerosol in springtime in Helsinki,
600 Finland. *J Aerosol Sci.*, 56, 61-77.

601 Verma, V., Fang, T., Xu, L., Peltier, R. E., Russell, A. G., Ng, N. L. & Weber, R. J. (2015) Organic
602 aerosols associated with the generation of reactive oxygen species (ROS) by water-soluble
603 PM2.5. *Environ. Sci. Technol.*, 49, 4646-56.

604 Vodicka, P., Kawamura, K., Schwarz, J. & Zdimal, V. (2022) Seasonal changes in stable carbon
605 isotopic composition in the bulk aerosol and gas phases at a suburban site in Prague. *Sci.*
606 *Total Environ.*, 803, 149767.

607 Wang, Y., Feng, Z., Yuan, Q., Shang, D., Fang, Y., Guo, S., Wu, Z., Zhang, C., Gao, Y., Yao, X.,
608 Gao, H. & Hu, M. (2023) Environmental factors driving the formation of water-soluble
609 organic aerosols: A comparative study under contrasting atmospheric conditions. *Sci. Total*
610 *Environ.*, 866, 161364.

611 Weber, R. J., Sullivan, A. P., Peltier, R. E., Russell, A., Yan, B., Zheng, M., de Gouw, J., Warneke,
612 C., Brock, C., Holloway, J. S., Atlas, E. L. & Edgerton, E. (2007) A study of secondary
613 organic aerosol formation in the anthropogenic-influenced southeastern United States. *J.*
614 *Geophys. Res. Atmos.*, 112.

615 Widory, D., Roy, S., Le Moullec, Y., Goupil, G., Cocherie, A. & Guerrot, C. (2004) The origin of
616 atmospheric particles in Paris: a view through carbon and lead isotopes. *Atmos. Environ.*, 38,
617 953-961.

618 Wong, J. P., Zhou, S. & Abbatt, J. P. (2015) Changes in secondary organic aerosol composition
619 and mass due to photolysis: relative humidity dependence. *J. Phys. Chem. A.*, 119, 4309-16.

620 Wu, Y., Huang, X., Jiang, Z., Liu, S. & Cui, L. (2020) Composition and sources of aerosol organic
621 matter in a highly anthropogenic influenced semi-enclosed bay: Insights from excitation-
622 emission matrix spectroscopy and isotopic evidence. *Atmos Res.*, 241.

623 Xiao, H. W., Xu, Y. & Xiao, H. Y. (2023) Source apportionment of black carbon aerosols in winter
624 across China. *Atmos. Environ.*, 298.

625 Xiao, R., Takegawa, N., Zheng, M., Kondo, Y., Miyazaki, Y., Miyakawa, T., Hu, M., Shao, M.,
626 Zeng, L., Gong, Y., Lu, K., Deng, Z., Zhao, Y. & Zhang, Y. H. (2011) Characterization and
627 source apportionment of submicron aerosol with aerosol mass spectrometer during the
628 PRIDE-PRD 2006 campaign. *Atmos. Chem. Phys.*, 11, 6911-6929.

629 Yao, P., Huang, R. J., Ni, H. Y., Kairys, N., Yang, L., Meijer, H. A. J. & Dusek, U. (2022) 13C
630 signatures of aerosol organic and elemental carbon from major combustion sources in China
631 compared to worldwide estimates. *Sci. Total Environ.*, 810.

632 Zaryab, A., Nassery, H. R., Knoeller, K., Alijani, F. & Minet, E. (2022) Determining nitrate
633 pollution sources in the Kabul Plain aquifer (Afghanistan) using stable isotopes and Bayesian
634 stable isotope mixing model. *Sci. Total Environ.*, 823.

635 Zhang, Y. L., Li, J., Zhang, G., Zotter, P., Huang, R. J., Tang, J. H., Wacker, L., Prevot, A. S. &
636 Szidat, S. (2014) Radiocarbon-based source apportionment of carbonaceous aerosols at a
637 regional background site on Hainan Island, South China. *Environ. Sci. Technol.*, 48, 2651-9.

638 Zhao, Y. L., Hennigan, C. J., May, A. A., Tkacik, D. S., de Gouw, J. A., Gilman, J. B., Kuster, W.
639 C., Borbon, A. & Robinson, A. L. (2014) Intermediate-volatility organic compounds: a large

640 source of secondary organic aerosol. *Environ. Sci. Technol.*, 48, 13743-13750.

641 Zhu, Q., He, L. Y., Huang, X. F., Cao, L. M., Gong, Z. H., Wang, C., Zhuang, X. & Hu, M. (2016)

642 Atmospheric aerosol compositions and sources at two national background sites in northern

643 and southern China. *Atmos. Chem. Phys.*, 16, 10283-10297.